2-2010

Exact calculation of entanglement in a 19-site two-dimensional spin system

Qing Xu
Purdue University - Main Campus, xu54@purdue.edu

Sabre Kais
Birck Nanotechnology Center and Department of Chemistry, Purdue University, kais@purdue.edu

Maxim Naumov
Purdue University - Main Campus, naumov@purdue.edu

Ahmed Sameh
Purdue University - Main Campus, sameh@purdue.edu

Exact calculation of entanglement in a 19-site two-dimensional spin system

Qing Xu,[1] Sabre Kais,[2,*] Maxim Naumov,[3] and Ahmed Sameh[3]
[1]*Department of Physics, Purdue University, West Lafayette, Indiana 47907, USA*
[2]*Department of Chemistry and Birck Nanotechnology Center, Purdue University, West Lafayette, Indiana 47907, USA*
[3]*Department of Computer Science, Purdue University, West Lafayette, Indiana 47907, USA*
(Received 22 September 2009; published 23 February 2010)

Using the trace minimization algorithm, we carried out an exact calculation of entanglement in a 19-site two-dimensional transverse Ising model. This model consists of a set of localized spin-$\frac{1}{2}$ particles in a two-dimensional triangular lattice coupled through exchange interaction J and subject to an external magnetic field of strength h. We demonstrate, for such a class of two-dimensional magnetic systems, that entanglement can be controlled and tuned by varying the parameter $\lambda = h/J$ in the Hamiltonian and by introducing impurities into the systems. Examining the derivative of the concurrence as a function of λ shows that the system exhibits a quantum phase transition at about $\lambda_c = 3.01$, a transition induced by quantum fluctuations at the absolute zero of temperature.

DOI: 10.1103/PhysRevA.81.022324 PACS number(s): 03.67.Mn, 05.30.−d, 03.65.Ud

I. INTRODUCTION

Entanglement, which is a quantum mechanical property that has no classical analog, has been viewed as a resource of quantum information and computation [1–8]. Intensive researches of entanglement measurement, entanglement monotone, criteria for distinguishing separable from entangled pure states and all the extensions from bipartite to multipartite systems have been carried out both qualitatively and quantitatively [1]. At the interface between quantum information and statistical mechanics, there has been particular analysis of entanglement in quantum critical models [9–12].

The critical properties in the entanglement allow for a screening of the qualitative change of the system and a deeper characterization of the ground-state wave function undergoing a phase transition. At $T = 0$, ground states of many-body systems contain all correlations concerning phases of matters. Traditionally, systems have been studied by looking, for example, at their external perturbations, various order parameters and excitation spectrum [1]. Methods developed from quantum information shed light on new ways of studying many-body systems [13–16], such as providing support for numerical calculations, like density matrix renormalization or design of new efficient simulation strategies for many-body systems.

Entanglement close to quantum phase transitions was originally analyzed by Osborne and Nielsen [10], and Osterloh *et al.* [9] for the Ising model in one dimension. Recently, we studied a set of localized spins coupled through exchange interaction and subject to an external magnetic field [17–20]. We demonstrated for such a class of one-dimensional (1D) magnetic systems, that entanglement can be controlled and tuned by varying the anisotropy parameter in the Hamiltonian and by introducing impurities into the systems. In particular, under certain conditions, the entanglement is zero up to a critical point λ_c, where a quantum phase transition occurs, and is different from zero above λ_c [21].

In two and higher dimensions nearly all calculations for spin systems were obtained by means of numerical simulations [22,23]. The concurrence and localizable entanglement in two-dimensional quantum *XY* and *XXZ* models were considered using quantum Monte Carlo simulations [24,25]. The results of these calculations were qualitatively similar to the one-dimensional case, but entanglement is much smaller in magnitude. Moreover, the maximum in the concurrence occurs at a position closer to the critical point than in the one-dimensional case [1].

The trace minimization algorithm for Hermitian eigenvalue problems, like those under consideration in this article, was introduced in 1982 by Sameh and Wisniewski [26]. It was designed specifically to handle very large problems on parallel computing platforms for obtaining the smallest eigenpairs. Later, a similar algorithm (Jacobi-Davidson) for the same eigenvalue problem was introduced by Sleijpen and Van der Vorst in 1996. A comparison of the two schemes by Sameh and Tong in [27] showed that the trace minimization scheme is more robust and efficient [28].

In this article, we use the trace minimization algorithm [26,27] to carry out an exact calculation of entanglement in a 19-site two-dimensional (2D) transverse Ising model. We classify the ground-state properties according to its entanglement for certain class on two-dimensional magnetic systems and demonstrate that entanglement can be controlled and tuned by varying the parameter $\lambda = h/J$ in the Hamiltonian and by introducing impurities into the systems. The article is organized as follows. In Sec. II, we give a brief overview of the model, entanglement of formation, and the trace minimization algorithm. Detailed methods are addressed in the appendix. We then proceed with the results and discussions of 1) the calculation of exact entanglement of a 19-site spin system, 2) the relationship of entanglement and quantum phase transition, and 3) the effects of impurities on the entanglement. The conclusions and the outlook are presented in the concluding section.

II. METHOD

A. Model

We consider a set of localized spin-$\frac{1}{2}$ particles in a two-dimensional triangular lattice coupled through exchange interaction J and subject to an external magnetic field of

*kais@purdue.edu

strength h. The Hamiltonian for such a system is given by

$$H = -\sum_{\langle i,j\rangle} J_{i,j}\sigma_i^x\sigma_j^x - h\sum_i \sigma_i^z, \tag{1}$$

where $\langle i, j\rangle$ is a pair of nearest-neighbor sites on the lattice, $J_{i,j} = J$ for all sites except the sites nearest to the impurity site i_m, while around the impurity site $J_{i,j} = (1+\alpha)J$, α measures the strength of the impurity that is located at site i_m, and σ_i^x and σ_i^z are the Pauli matrices. For this model it is convenient to define a dimensionless coupling constant $\lambda = h/J$.

B. Entanglement of formation

We confine our interest to the entanglement of two spins, at any position i and j [9]. We adopt the entanglement of formation, a well-known measure of entanglement [29], to quantify our entanglement [21]. All the information needed in this case is contained in the reduced density matrix $\rho_{i,j}$. Wootters [29] has shown, for a pair of binary qubits, that the concurrence C, which goes from 0 to 1, can be taken as a measure of entanglement. The concurrence between sites i and j is defined as [29]

$$C(\rho) = \max\{0, \epsilon_1 - \epsilon_2 - \epsilon_3 - \epsilon_4\}, \tag{2}$$

where the ϵ_i's are the eigenvalues of the Hermitian matrix $R \equiv \sqrt{\sqrt{\rho}\tilde{\rho}\sqrt{\rho}}$ with $\tilde{\rho} = (\sigma^y \otimes \sigma^y)\rho^*(\sigma^y \otimes \sigma^y)$ and σ^y is the Pauli matrix of the spin in y direction. For a pair of qubits the entanglement can be written as,

$$E(\rho) = \epsilon\big(C(\rho)\big), \tag{3}$$

where ϵ is a function of the "concurrence" C,

$$\epsilon(C) = h\left(\frac{1+\sqrt{1-C^2}}{2}\right), \tag{4}$$

where h is the binary entropy function,

$$h(x) = -x\log_2 x - (1-x)\log_2(1-x). \tag{5}$$

In this case, the entanglement of formation is given in terms of another entanglement measure, the concurrence C. The entanglement of formation varies monotonically with the concurrence.

The matrix elements of the reduced density matrix needed for calculating the concurrence are obtained numerically using the formalism developed in the following section.

C. Trace minimization algorithm

Diagonalizing a 2^{19} by 2^{19} Hamiltonian matrix and partially tracing its density matrix is a numerically difficult task. We propose to compute the entanglement of formation, first by applying the trace minimization algorithm (Tracemin) [26,27] to obtain the eigenvalues and eigenvectors of the constructed Hamiltonian. Then, we use these eigenpairs and new techniques detailed in the appendix to build partially traced density matrix.

The trace minimization algorithm was developed for computing a few of the smallest eigenvalues and the corresponding eigenvectors of the large sparse generalized eigenvalue problem

$$AU = BU\Sigma, \tag{6}$$

where matrices $A, B \in \mathbb{C}^{n\times n}$ are Hermitian positive definite, $U = [u_1, \ldots, u_p] \in \mathbb{C}^{n\times p}$, and $\Sigma \in \mathbb{R}^{p\times p}$ is a diagonal matrix. The main idea of Tracemin is that minimizing $\mathrm{Tr}(X^*AX)$, subject to the constraints $X^*BX = I$, is equivalent to finding the eigenvectors U corresponding to the p smallest eigenvalues. This consequence of the Courant-Fischer theorem can be restated as

$$\min_{X^*BX=I} \mathrm{Tr}(X^*AX) = \mathrm{Tr}(U^*AU) = \sum_{i=1}^{p}\lambda_i, \tag{7}$$

where I is the identity matrix. The following steps constitute a single iteration of the Tracemin algorithm:

$G = X_k^*BX_k$	(compute G)
$G = V\Omega V^*$	(compute the spectral decomposition of G)
$H = \tilde{Q}^*A\tilde{Q}$	(compute H, where $\tilde{Q} = X_kV\Omega^{-1/2}$)
$H = W\Omega W^*$	(compute the spectral decomposition of H)
$\bar{X}_k = \tilde{Q}W$	(now $\bar{X}_k^*A\bar{X}_k = \Lambda$ and $\bar{X}_k^*B\bar{X}_k = I$)
$\bar{X}_{k+1} = \bar{X}_k - D$	[D is determined $\mathrm{Tr}(X_{k+1}^*AX_{k+1}) < \mathrm{Tr}(X_k^*AX_k)$].

In order to find the optimal update D in the last step, we enforce the natural constraint $\bar{X}_k^*BD = 0$, and obtain

$$\begin{pmatrix} A & B\bar{X}_k \\ X_k^*B & 0 \end{pmatrix}\begin{pmatrix} D \\ L \end{pmatrix} = \begin{pmatrix} A\bar{X}_k \\ 0 \end{pmatrix}. \tag{8}$$

Considering the orthogonal projector $P = B\bar{X}_k(X_k^*B^2X_k)^{-1}\bar{X}_k^*B$ and letting $D = (I-P)\bar{D}$, the linear system Eq. (8) can be rewritten in the following form

$$(I-P)A(I-P)\bar{D} = (I-P)A\bar{X}_k. \tag{9}$$

Notice that the conjugate gradient method can be used to solve Eq. (9), since it can be shown that the residual and search directions $r, p \in \mathrm{Range}(P)^{\perp}$. Also, notice that the linear system Eq. (9) need to be solved only to a fixed relative precision at every iteration of Tracemin.

A reduced density matrix, built from the ground state, which is obtained by Tracemin, is usually constructed as follows: diagonalize the system Hamiltonian $H(\lambda)$, retrieve the ground state $|\Psi\rangle$ as a function of $\lambda = h/J$, build the density matrix $\rho = |\Psi\rangle\langle\Psi|$, and trace out contributions of all the other spins in density matrix to get reduced density matrix by $\rho(i,j) = \sum_p \langle u_i(A)|\langle v_p(B)|\rho|u_j(A)\rangle|v_p(B)\rangle$, where $u_i(A)$ and $v_p(B)$ are bases of subspaces $\epsilon(A)$ and $\epsilon(B)$. That includes creating a $2^{19}\times 2^{19}$ density matrix ρ followed by permutations of rows, columns, and some basic arithmetic operations on the elements of ρ. Instead of operating on a huge matrix, we pick up only certain elements from $|\Psi\rangle$, performing basic algebra to build a reduced density matrix directly. Details are in the appendix.

III. RESULTS AND DISCUSSIONS

A. Exact entanglement of a 19-site spin system

We examine the change of concurrence in Eq. (2) between the center spin and its nearest neighbor as a function of $\lambda = h/J$ for both the 7-site and 19-site systems. In Fig. 1, the concurrence of the 7-site system reaches its maximum 0.15275 when $\lambda = 2.61$. In the 19-site system, the concurrence reaches

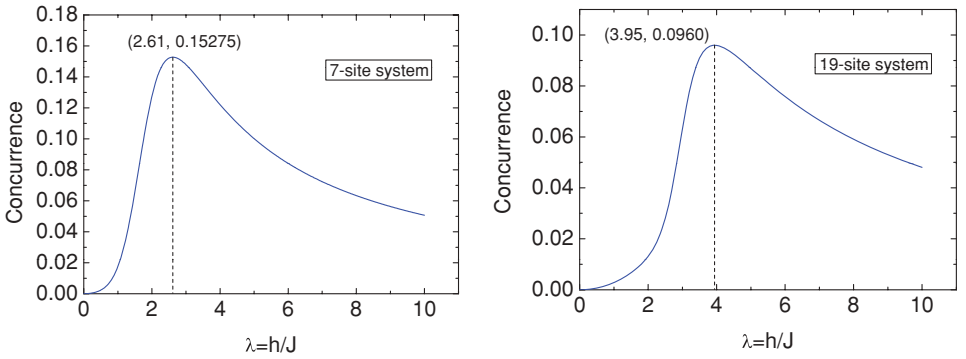

FIG. 1. (Color online) Concurrence of center spin and its nearest neighbor as a function of λ for both the 7-site and 19-site systems. In the 7-site system, concurrence reaches the maximum 0.15275 when $\lambda = 2.61$. In the 19-site system, concurrence reaches the maximum 0.0960 when $\lambda = 3.95$.

0.0960 when $\lambda = 3.95$. The maximum value of concurrence in the 19-site model, where each site interacts with six neighbors, is roughly one-third of the maximum concurrence in the one-dimensional transverse Ising model with size $N = 201$ [17], where it has only two neighbors for each site. It is the monogamy [30,31] that limits the entanglement shared among the number of neighboring sites.

However, entanglement between other nearest neighbors are slightly different than those between the pairs involving the center. Figure 2 shows that the fewer the number of neighbors of a pair the larger the entanglement. The concurrence between the first and second spins is greater than that between the first and fourth in the 7-site system. For the 19-site system, the concurrence between the first and second spins is greater than that between the second and fifth. The same rule applies to the others, therefore $C_{2,5} > C_{5,6} > C_{5,10}$. Although 5 and 6, and 5 and 10, have the same number of neighbors, the number of neighbors of neighbors of 5 and 6 is less than that of 5 and 10. Consequently, $C_{5,6}$ is slightly larger than $C_{5,10}$.

Our numerical calculation shows that the maximum concurrence of next-nearest neighbor (say the 1st and 10th spins) is less than 10^{-8}. The truly nonlocal quantum part of the two-point correlations is nonetheless very short ranged [9]. It shows that the entanglement is short ranged, though global. These results are similar to those obtained for Ising one-dimensional spin systems in a transverse magnetic field [9]. The range of entanglement, that is, the maximum distance between two spins at which the concurrence is different from zero, is short. The concurrence vanishes unless the two sites are at most next neighbors.

B. Entanglement and quantum phase transition

As we mentioned in Sec. II B, all the information needed for quantifying the entanglement of two spins is contained in the reduced density matrix obtained from density matrix. In other words, entanglement is coded by the information of ground state, while the quantum phase transition is characterized by the change of ground state. In order to quantify the change of the many-body wave function when the system crosses the critical point, we calculate the change of concurrence $dC/d\lambda$ between the center and its nearest neighbor as a function of parameter λ for both 7- and 19-site systems, as shown in Fig. 3. It is known that an infinite system—a system at the thermodynamic limit—is supposed to have a singularity at the critical point of quantum phase transition; for a finite system one still has to take finite-size effect into consideration. However, in Fig. 3 both systems show strong tendency of being singular at $\lambda_c = 1.64$ and $\lambda_c = 3.01$, respectively. Renormalization group method for an infinite triangular system predicts critical point at $\lambda_c = 4.75784$; the same method for a square lattice system at $\lambda_c = 2.62975$ [33], while finite-size scaling has $\lambda_c = 3.044$ for square lattice [34]. Our results show that the tendency to be singular is moving toward the infinite critical point as the size increases. For one-dimensional systems, since the calculations can be done for a large number of spins, finite-size scaling calculations for N ranging from 41 to 401 spins indicate that the derivative of the concurrence diverges logarithmically with increasing system size [9]. In our study we cannot perform finite-size scaling analyses since we do not have enough data points to perform data collapse [35]. Optimization methods [36] and

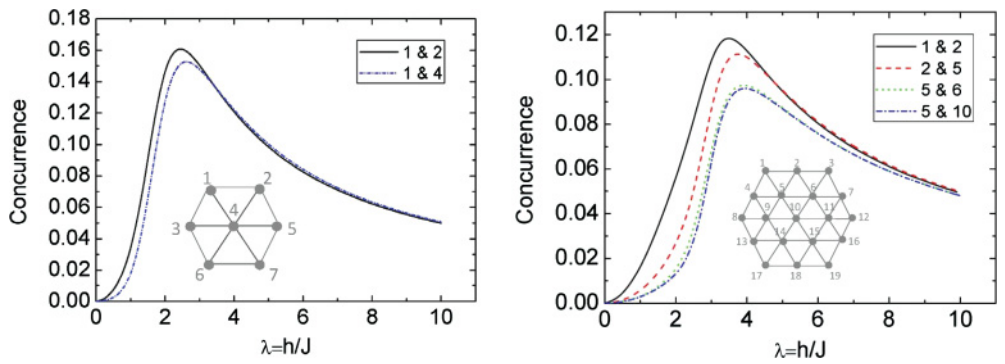

FIG. 2. (Color online) The nearest neighbor concurrence as a function of λ for different pairs. In the 7-site system, there are two distinct pairs 1 and 2, and 1 and 4. In the 19-site system, they are 1 and 2, 2 and 5, 5 and 6, and 5 and 10.

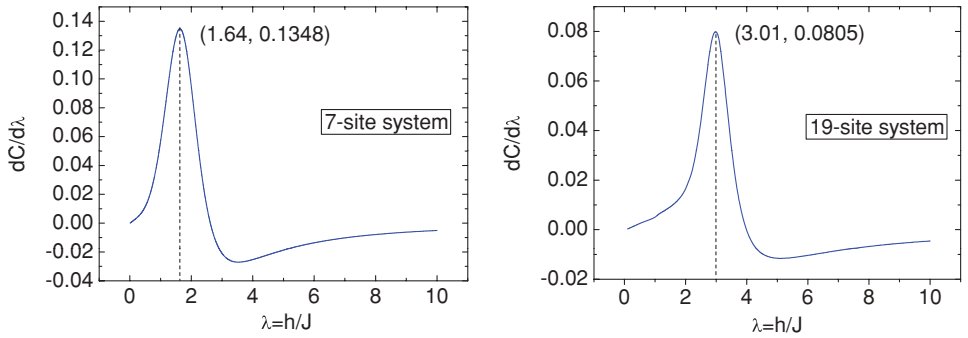

FIG. 3. (Color online) The change of concurrence between the center and its nearest neighbor as a function of parameter λ for the 7-site and 19-site systems, respectively. They both show the strong tendency of singularity at $\lambda = 1.54$ and $\lambda = 3.01$.

parallel Tracemin code is under development, which will allow us to obtain exact results for larger systems.

To understand this model better, a discussion about the degeneracy in the system and an explanation of the energy spectrum is necessary. It is known that the ground-state degeneracy of the Heisenberg spin model depends on whether the total number of spins is even (singlet) or odd (doublet). For the Ising model with transverse field on an infinite 1D chain, the ground state in the ferromagnetic (FM) phase is doubly degenerate and is gaped from the excitation spectrum by $2J(1 - h/J)$ [37]. (Note, however, that this degeneracy is never achieved unless one goes to the thermaldynamic limit, regardless of the number of spins being even or odd.) In our model, the Ising coupling is ferromagnetic, as opposed to the spin liquid case with antiferromagnetic coupling, and the system is expected to break the Z_2 symmetry and develop the (Ising) FM order under the small transverse field. Further, due to the construction of the lattice, it is impossible to have a system that has an even number of sites while conserving all the lattice group symmetries. So we expect that the same doublet degeneracy remains 2D as the system goes to the thermaldynamic limit. The energy gaps from our numerical results of finite systems are less than 10^{-8} (Fig. 4), which are well consistent with the expectation. The strict doublets in finite systems only happen at $h/J = 0$ exactly, when entanglements naturally are zero, not entangled at all; no matter which one of the doublet ground state is chosen, it gives the same value of entanglement. Otherwise even a very small h helps distinguish the ground state. Technically, we do not have to worry that a different superposition of the ground states gives different values of entanglement.

The energy separation between the ground state and the first excited state in terms of λ clarifies the spectrum of the system. Figure 4 presents the doublet degeneracy of the ground state and they separate around $\lambda = 1.5$ for the 7-site and $\lambda = 2.5$ for the 19-site system. While in the $dC/d\lambda$ versus λ graph, both systems show strong tendency of being singular at $\lambda_c = 1.64$ and $\lambda_c = 3.01$, respectively. Both "separation position" and "singular position" are used as an indicator of "critical point." And we believe using the finite-size scaling method will also give the same "critical point" of the infinite system. But it seems $dC/d\lambda$ versus λ is a better indicator because for the same size system it points out a value closer to the expected critical point. This property benefits the finite-size scaling method, since fewer and/or smaller systems may be needed.

C. Introducing impurities to tune the entanglement

We introduce one impurity in the center of the 19-site spin system. The impurity only interacts with nearest neighbors in strength $J' = (1 + \alpha)J$. When the strength increases, the concurrence of any two spins decreases. Then we move the impurity to site 5. The concurrence shows the same trend of decreasing, as the impurity strengths go up. Details are shown in Fig. 5 for the concurrence of different pairs with various strength of impurity in the center of the 7-site system, while Fig. 6 shows the results for 19-site system. Figure 7 shows the results with various strength of impurity at site 1 of a 7-site system and Fig. 8 for various strength of impurity at site 5 of a 19-site system.

The maximum of entanglement is shifted with the increasing of the parameter α. The shift is the result of the competition between the spin-spin interaction J and the external transverse magnetic field h. Consider the ideal situation of pure infinite system. Without the coupling interaction, all the spins will point along the direction of transverse field. While with the absence of a transverse field, the ground state is supposed to be twofold degenerated, either along the positive x direction or the negative x direction. Every spin has six neighbors, so averagely is affected by three J and one h. When the two forces are well matched in strength, the phase transition occurs.

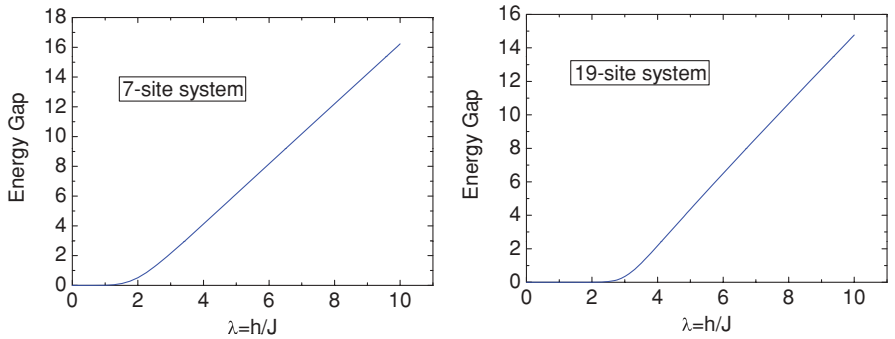

FIG. 4. (Color online) The energy separation between the ground state and the first excited state as a function of λ.

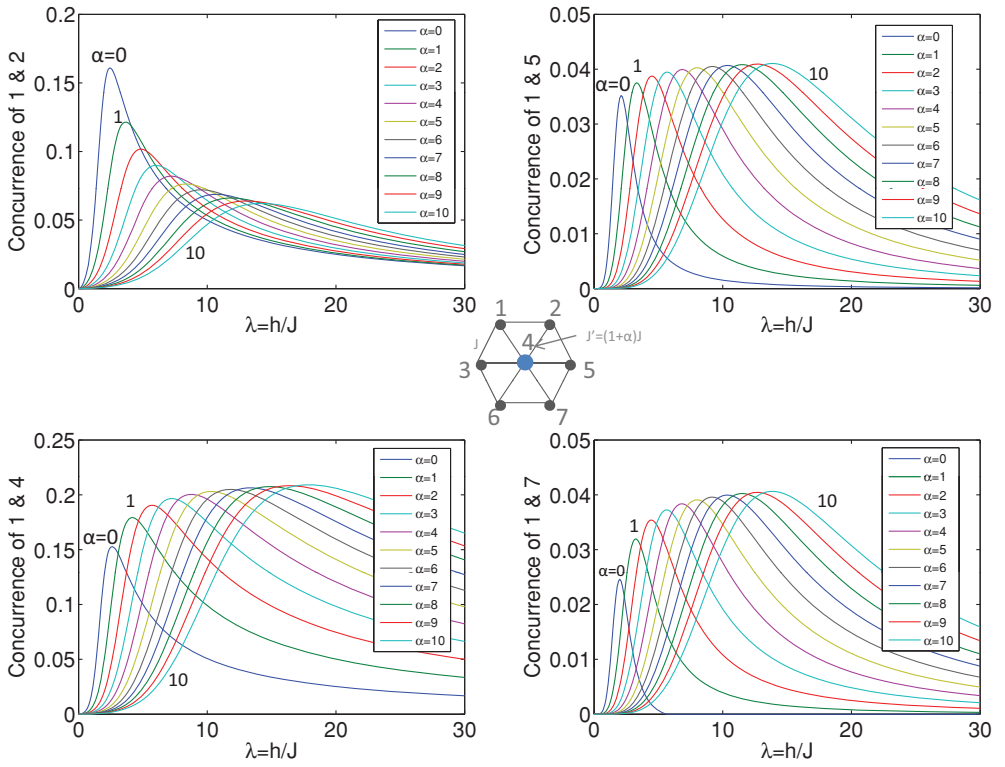

FIG. 5. (Color online) Concurrences of different pairs with various strength of impurity in the center of the 7-site system. Curves shown top to bottom in legend are shown from left to right in figure.

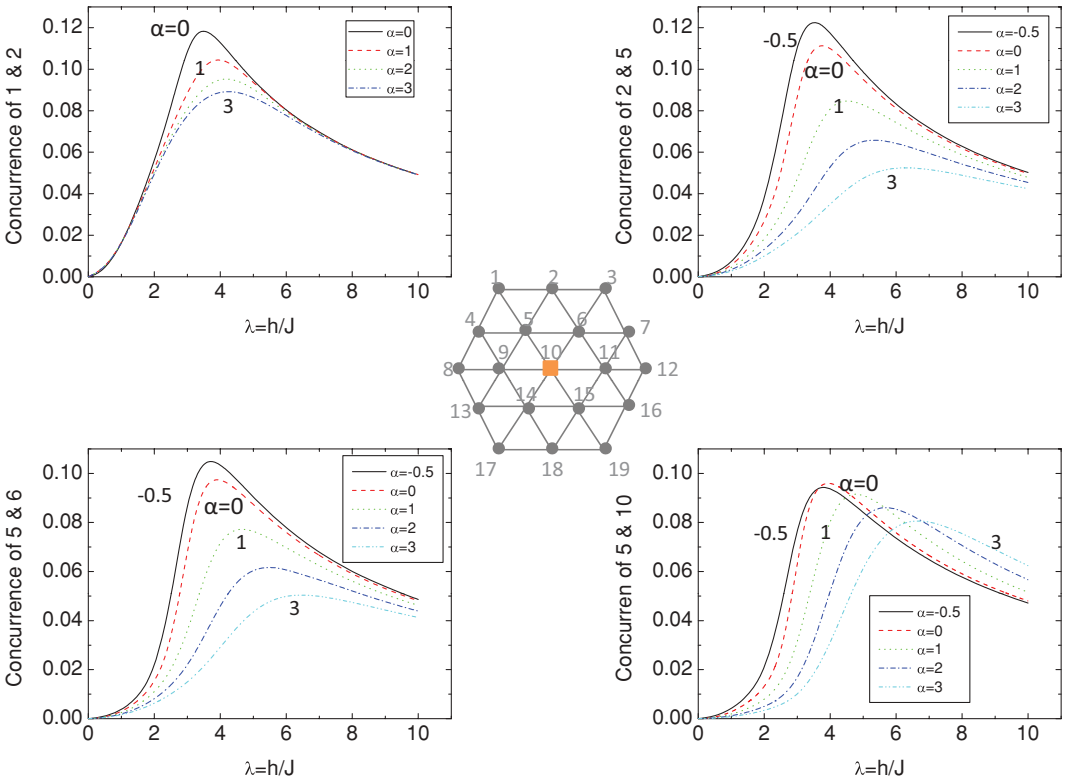

FIG. 6. (Color online) Concurrence of different pairs with various strength of impurity in the center of the 19-site system.

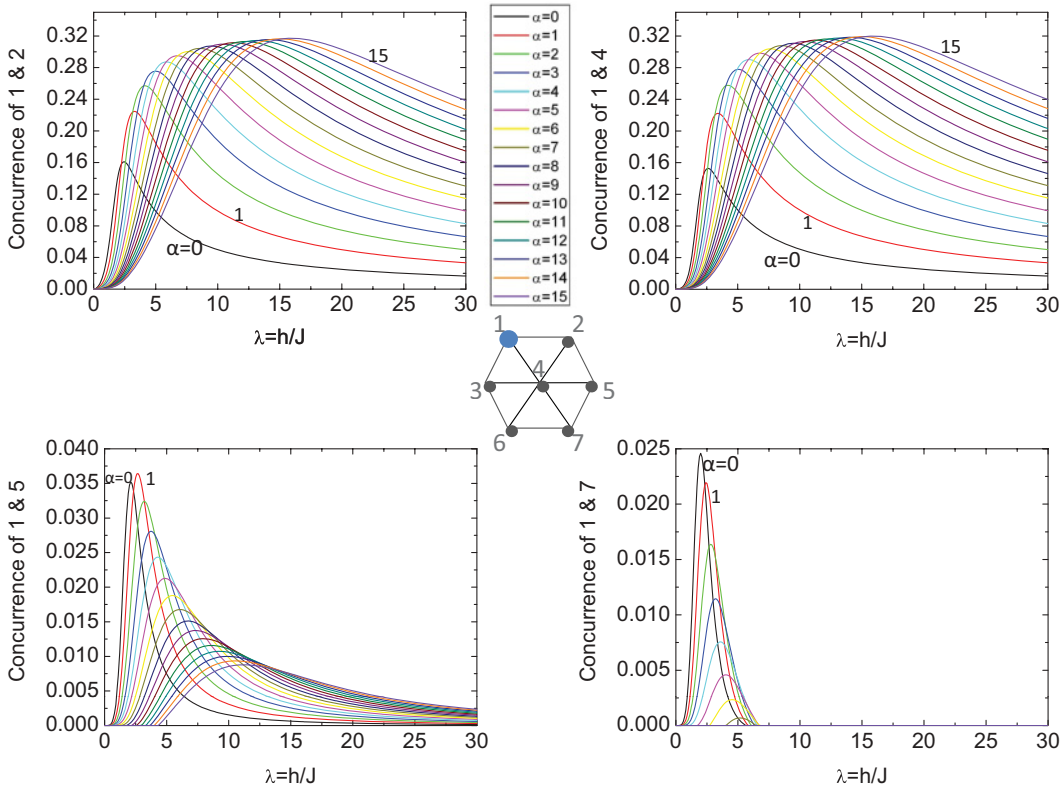

FIG. 7. (Color online) Concurrence of different pairs with various strength of impurity at site 1 of a 7-site system. Curves shown from top to bottom in legends are shown from left to right in figure.

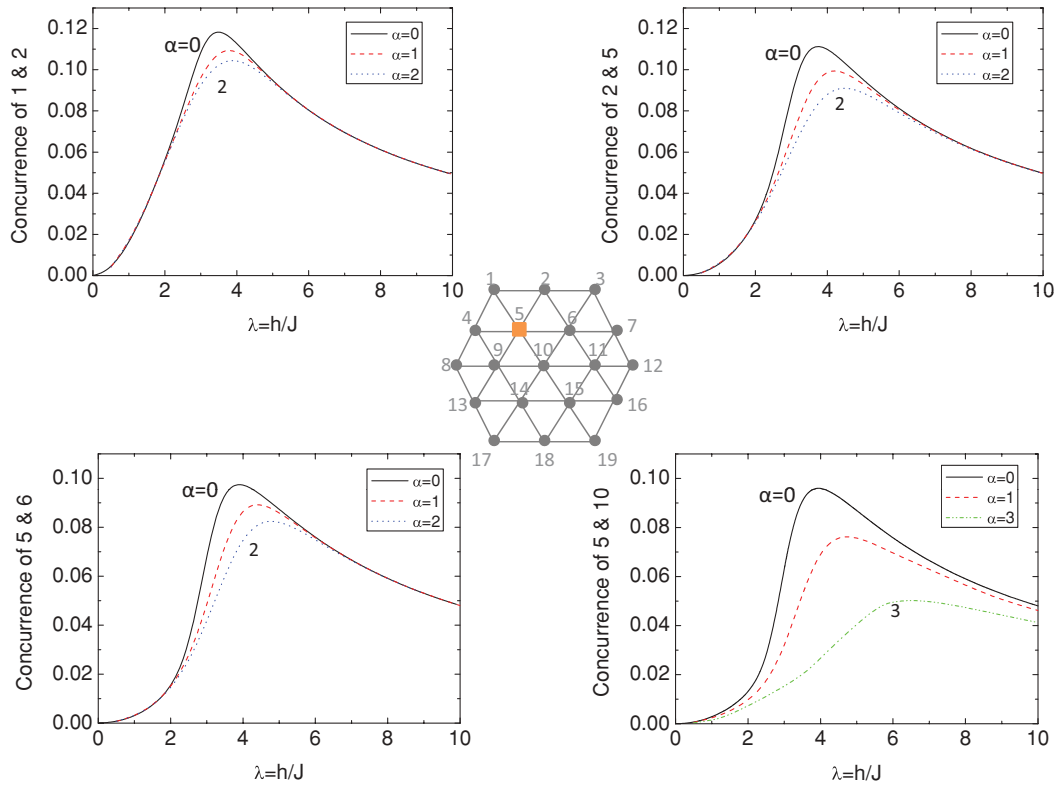

FIG. 8. (Color online) Concurrence of different pairs with various strength of impurity at site 5 of a 19-site system.

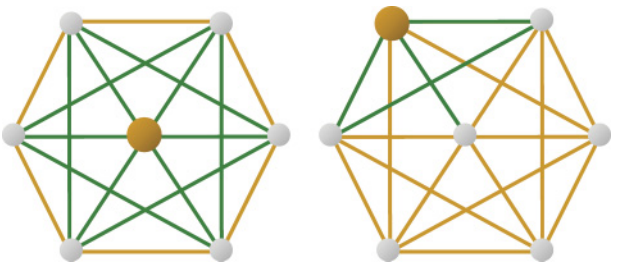

FIG. 9. (Color online) Overview of the change of concurrence in the 7-site system. The large yellow dot stands for the impurity and silver dots denote regular spins. Lines connecting two sites represent the entanglement. If the line is green, it means the entanglement between two sites increases as the impurity gets "stronger"; otherwise the yellow line indicates that the entanglement decreases when the impurity increases.

Figure 3 indicates the 19-site system has a strong tendency of singularity at $\lambda = 3.01$, which is consistent and very close with the above statement. When the system is finite, the boundary effect (less than six neighbors) will affect the position of the maximum of entanglement a little bit as Fig. 2 shows for different pairs. After we introduce the impurity, the balance of 3 : 1 is destroyed, so the maximum of entanglement is shifted quite a bit for a different strength of $J' = (1 + \alpha)J$.

The value of the maximum changes with α is because of the monogamy that limits the entanglement shared among neighbors. For example, in Fig. 4, the stronger the interactions between 1 and 4, and 2 and 4 (i.e., the larger α, the less 1 and 2 entangle). Therefore, the value of maximum decreases for the larger α.

Figure 9 gives a good overview of the change of concurrence for the 7-site system. The large yellow dot stands for the impurity and silver dots denote regular spins. Lines connecting two sites represent the entanglement. If the line is green, it means the entanglement between two sites increases as the impurity gets "stronger," and the yellow line indicates that the entanglement decreases when the impurity increases. We can explain these phenomena of the 7-site system as follows. When the impurity interacts more with the neighbor, the pair also entangles more. Since some spins are more involved with the impurity, they themselves entangle less. The only exceptions are the next-nearest neighbors. Thus, entanglement close to the impurity tends to get bigger when J' is greater than J. However, the behavior of entanglement between sites 5 and 10 in the 19-site system surprisingly goes down as the strength of the impurity coupling increases. It is not clear why the behavior is different for the one in the 7-site system and whether increasing the system size has any effect. We are planning to increase the size of the system to include the next layer, which will bring the system to 37 sites, in order to analyze this phenomena.

All the results above are obtained through sequential computing. In the future, to increase the object size under consideration, we plan to take advantage of parallel computing. We already have a parallel Tracemin algorithm and we are developing a parallel code for computation of the partial trace. This will be useful as we expand our 2D systems to a larger number of spins in order to perform finite-size scaling for quantum critical parameters.

In summary, the Tracemin algorithm allowed us to carry out an exact calculation of entanglement in a 19-site two-dimensional transverse Ising model. We demonstrated for such a class of two-dimensional magnetic systems that entanglement can be controlled and tuned by varying the parameter λ in the Hamiltonian and by introducing impurities into the systems.

ACKNOWLEDGMENTS

We thank the Army Research Office (ARO) and the Binational Science Foundation (BSF) for financial support.

APPENDIX A: APPLICATIONS OF TRACE MINIMIZATION ALGORITHM

1. General forms of matrix representation of the Hamiltonian

By studying the patterns of $\sum_{\langle i,j\rangle} I \otimes \cdots \sigma_i^x \otimes \cdots \sigma_j^x \otimes \cdots I$ and $\sum_i I \otimes \cdots \sigma_i^z \otimes \cdots I$, one finds the following rules.

a. $\sum_i \sigma_i^z$ *for N spins*

The matrix is 2^N by 2^N; it has only 2^N diagonal elements. Elements follow the rules shown in Fig. 10.

If one stores these numbers in a vector, and initializes $v = (N)$, then the new v is the concatenation of the original v and the original v with 2 subtracted from each of its elements. We repeat this N times, that is,

$$v = \begin{pmatrix} v \\ v-2 \end{pmatrix}; \tag{A1}$$

$$v = (N), \tag{A2}$$

$$\Rightarrow v = \begin{pmatrix} N \\ N-2 \end{pmatrix}, \tag{A3}$$

$$\Rightarrow v = \begin{pmatrix} N \\ N-2 \\ N-2 \\ N-4 \end{pmatrix}. \tag{A4}$$

b. $\sum_{\langle i,j\rangle} I \otimes \cdots \sigma_i^x \otimes \cdots \sigma_j^x \otimes \cdots I$ *for N spins*

Since $\left(\begin{smallmatrix} 1 & 0 \\ 0 & 1 \end{smallmatrix}\right)$ and $\left(\begin{smallmatrix} 0 & 1 \\ 1 & 0 \end{smallmatrix}\right)$ exclude each other, for matrix $I \otimes \cdots \sigma_i^x \otimes \cdots \sigma_j^x \otimes \cdots I$, every row or column contains only

Scheme		Rule	Example N=3
N		N	3
N-2		N-2	1
N	-2	N-2	1
N-2	-2	N-4	-1
N	-2	N-2	1
N-2	-2	N-4	-1
N-2	-2	N-4	-1
N-4	-2	N-6	-3
and so on		and so on	

FIG. 10. Diagonal elements of $\sum_i \sigma_i^z$ for N spins.

one "1," then the matrix owns 2^N "1"s and only "1" in it. If we know the position of "1"s, it turns out that we can set a 2^N by 1 array "col" to store the column position of "1"s corresponding to the 1st $\rightarrow$ 2^Nth rows. In fact, the nonzero elements can be located by the properties stated below. For clarity, let us number N spins in the reverse order as: N-1, N-2, ... , 0, instead of 1, 2, ... , N. The string of nonzero elements starts from the first row at: $1 + 2^i + 2^j$; with string length 2^j; and number of such strings 2^{N-j-1}. For example, Fig. 11 shows these rules for a scheme of $I \otimes \sigma_3^x \otimes \sigma_2^x \otimes I \otimes I$.

Again, because of the exclusion, the positions of nonzero element "1" of $I \otimes \cdots \sigma_i^x \otimes \cdots \sigma_j^x \otimes \cdots I$ are different from those of $I \otimes \cdots \sigma_l^x \otimes \cdots \sigma_m^x \otimes \cdots I$. So $\sum_{\langle i,j\rangle} I \otimes \cdots \sigma_i^x \otimes \cdots \sigma_j^x \otimes \cdots I$ is a 2^N by 2^N matrix with only 1 and 0.

After storing array "col," we repeat the algorithm for all the nearest pairs $\langle i, j\rangle$, and concatenate "col"s to position matrix "c" of $\sum_{\langle i,j\rangle} I \otimes \cdots \sigma_i^x \otimes \cdots \sigma_j^x \otimes \cdots I$. In the next section we apply these rules to our problem.

2. Specialized matrix multiplication

Using the diagonal elements array "v" of $\sum_i \sigma_i^z$ and position matrix of nonzero elements "c" for $\sum_{\langle i,j\rangle} I \otimes \cdots \sigma_i^x \otimes \cdots \sigma_j^x \otimes \cdots I$, we can generate matrix H, representing the Hamiltonian. However, we only need to compute the result of the matrix-vector multiplication $H \times Y$ in order to run Tracemin, which is the advantage of Tracemin, and consequently do not need to explicitly obtain H. Since matrix-vector multiplication is repeated many times throughout iterations, we propose an efficient implementation to speed up its computation specifically for Hamiltonian of Ising model (and XY by adding one term).

For simplicity, first let Y in $H \times Y$ be a vector and $J = h = 1$ (in general Y is a tall matrix and $J \neq h \neq 1$). Then

$$
\begin{aligned}
H \times Y &= \sum_{\langle i,j\rangle} \sigma_i^x \sigma_j^x \times Y + \sum_i \sigma_i^z \times Y \\
&= \begin{pmatrix} 1 & 1 & 1 & \\ & 1 & 1 & 1 \\ \cdots & \cdots & & \\ & & & \\ \cdots & \cdots & & \\ 1 & & & 1\ 1 \end{pmatrix} \times \begin{pmatrix} Y(1) \\ Y(2) \\ \vdots \\ \vdots \\ Y(2^N) \end{pmatrix} + \begin{pmatrix} v(1) & & & \\ & v(2) & & \\ & & \ddots & \\ & & & \ddots \\ & & & v(2^N) \end{pmatrix} \times \begin{pmatrix} Y(1) \\ Y(2) \\ \vdots \\ \vdots \\ Y(2^N) \end{pmatrix} \\
&= \begin{pmatrix} Y(c(1,1)) + Y(c(1,2)) + \cdots + Y(c(1,p_\#)) \\ \vdots \\ Y(c(k,1)) + Y(c(k,2)) + \cdots + Y(c(k,p_\#)) \\ \vdots \\ Y(c(2^N,1)) + Y(c(2^N,2)) + \cdots + Y(c(2^N,p_\#)) \end{pmatrix} + \begin{pmatrix} v(1) \times Y(1) \\ v(2) \times Y(2) \\ \vdots \\ \vdots \\ v(2^N) \times Y(2^N) \end{pmatrix},
\end{aligned} \tag{A5}
$$

where $p_\#$ stands for the number of pairs.

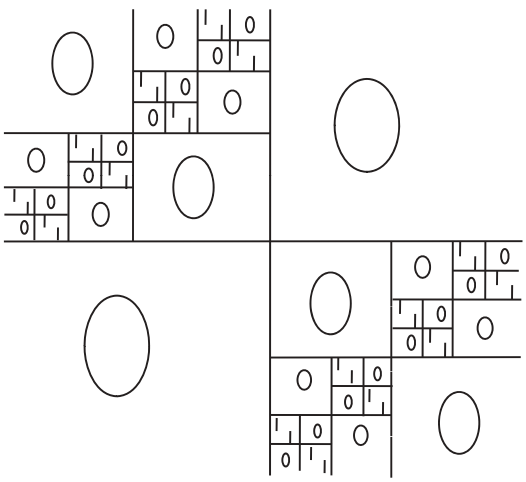

FIG. 11. Scheme of matrix $I \otimes \sigma_3^x \otimes \sigma_2^x \otimes I \otimes I$.

When Y is a matrix, we can treat ($Y2^N$ by p) column by column for $\sum_{\langle i,j\rangle} I \otimes \cdots \sigma_i^x \otimes \cdots \sigma_j^x \otimes \cdots I$. Also, we can accelerate the computation by treating every row of Y as a vector and adding these vectors at once. Figure 12 visualized the process.

Notice that the result of the multiplication of the xth row of $\sum_{\langle i,j\rangle} \sigma_i^x \sigma_j^x$ (delineated by the left box in figure 12 below) and Y, is equivalent to the sum of rows of Y, whose row numbers are the column indices of nonzero elements of the xth row, such that we transform a matrix operation to straightforward summation and multiplication of numbers.

APPENDIX B: PARTIAL TRACE

All the information needed for quantifying the entanglement of two spins i and j is contained in the reduced density matrix $\rho(i, j)$, which can be obtained from global density matrix $\rho = |\psi\rangle\langle\psi|$, where $|\psi\rangle$ is the ground state of the system, via partial trace. Now let us show how we can obtain the reduced density matrix from the ground state calculated by Tracemin.

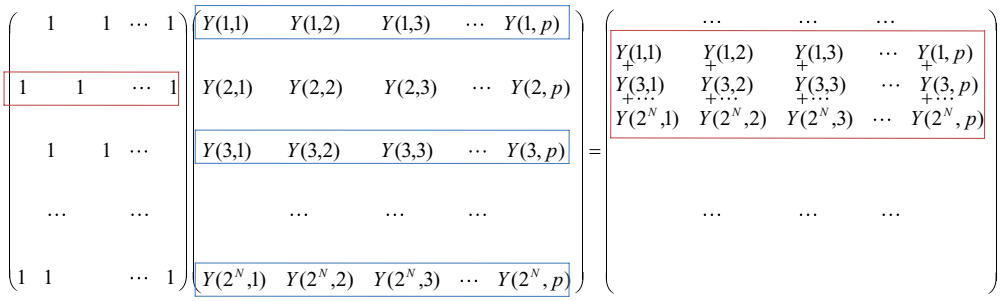

FIG. 12. (Color online) Illustration of $H \times Y$.

1. Density operator in the pure case and partial trace

Consider a system whose state vector at the instant t is

$$|\psi(t)\rangle = \sum_n c_n(t)|u_n\rangle, \quad \sum_n |c_n(t)|^2 = 1. \tag{B1}$$

The density operator $\rho(t)$ is defined as

$$\rho(t) = |\psi(t)\rangle\langle\psi(t)|. \tag{B2}$$

It enables us to obtain all the physical predictions of an observable $A(t)$ by

$$\langle A(t)\rangle = \mathrm{Tr}\{\rho(t)A\}. \tag{B3}$$

Let us consider two different systems (1) and (2) and the global system (1) + (2), whose state space is the tensor product: $\varepsilon = \varepsilon(1) \otimes \varepsilon(2)$. Let $|u_n(1)\rangle$ be a basis of $\varepsilon(1)$ and $|v_p(2)\rangle$, a basis of $\varepsilon(2)$, the kets $|u_n(1)\rangle|v_p(2)\rangle$ from a basis of ε.

The density operator ρ of the global system is an operator that acts in ε. We construct from ρ an operator $\rho(1)$ [or $\rho(2)$] acting only in $\varepsilon(1)$ [or $\varepsilon(2)$], which will enable us to make all the physical predictions about measurements bearing only on system (1) or system (2). This operation will be called a partial trace with respect to (2) [or (1)]. Matrix elements of the operator $\rho(1)$ are

$$\langle u_n(1)|\rho(1)|u_{n'}(1)\rangle = \sum_p (\langle u_n(1)|\langle v_p(2)|)\rho(|u_{n'}(1)\rangle|v_p(2)\rangle). \tag{B4}$$

Now let $A(1)$ be an observable acting in $\varepsilon(1)$ and $\widetilde{A}(1) = A(1) \otimes I(2)$, its extension in ε. We obtain, using the definition of the trace and closure relation,

$$\widetilde{A}(1)\rangle = \mathrm{Tr}\{\rho(1)A(1)\}. \tag{B5}$$

As it is designed, the partial trace $\rho(1)$ enables us to calculate all the mean values $\langle\widetilde{A}(1)\rangle$ as if the system(1) were isolated and had $\rho(1)$ for a density operator [32].

2. Properties of the reduced density matrix

As we calculate the entanglement of formation, we trace out all spins but two (bipartite). Their reduced density matrix is, therefore, four by four. Reality and parity conservation of H together with translational invariance already fix the structure of ρ to be symmetric with ρ_{11}, ρ_{22}, ρ_{33}, ρ_{44}, ρ_{14}, ρ_{23} as the only nonzero entries. It follows from the symmetry properties of the Hamiltonian, the ρ must be real and symmetrical, plus the global phase flip symmetry of Hamiltonian, which implies that $[\sigma_i^z\sigma_j^z, \rho_{ij}] = 0$, so

$$\begin{pmatrix} 1 & & & \\ & -1 & & \\ & & -1 & \\ & & & 1 \end{pmatrix} \begin{pmatrix} \rho_{11} & \rho_{12} & \rho_{13} & \rho_{14} \\ \rho_{21} & \rho_{22} & \rho_{23} & \rho_{24} \\ \rho_{31} & \rho_{32} & \rho_{33} & \rho_{34} \\ \rho_{41} & \rho_{42} & \rho_{43} & \rho_{44} \end{pmatrix} - \begin{pmatrix} \rho_{11} & \rho_{12} & \rho_{13} & \rho_{14} \\ \rho_{21} & \rho_{22} & \rho_{23} & \rho_{24} \\ \rho_{31} & \rho_{32} & \rho_{33} & \rho_{34} \\ \rho_{41} & \rho_{42} & \rho_{43} & \rho_{44} \end{pmatrix} \begin{pmatrix} 1 & & & \\ & -1 & & \\ & & -1 & \\ & & & 1 \end{pmatrix} = 0, \tag{B6}$$

$$\begin{pmatrix} \rho_{11} & \rho_{12} & \rho_{13} & \rho_{14} \\ -\rho_{21} & -\rho_{22} & -\rho_{23} & -\rho_{24} \\ -\rho_{31} & -\rho_{32} & -\rho_{33} & -\rho_{34} \\ \rho_{41} & \rho_{42} & \rho_{43} & \rho_{44} \end{pmatrix} - \begin{pmatrix} \rho_{11} & -\rho_{12} & -\rho_{13} & \rho_{14} \\ \rho_{21} & -\rho_{22} & -\rho_{23} & \rho_{24} \\ \rho_{31} & -\rho_{32} & -\rho_{33} & \rho_{34} \\ \rho_{41} & -\rho_{42} & -\rho_{43} & \rho_{44} \end{pmatrix} = 0, \tag{B7}$$

$$2\begin{pmatrix} 0 & \rho_{12} & \rho_{13} & 0 \\ -\rho_{21} & 0 & 0 & -\rho_{24} \\ -\rho_{31} & 0 & 0 & -\rho_{34} \\ 0 & \rho_{42} & \rho_{43} & 0 \end{pmatrix} = 0, \tag{B8}$$

$$\rho_{12} = \rho_{13} = \rho_{21} = \rho_{24} = \rho_{31} = \rho_{34} = 0. \tag{B9}$$

Because ρ_{ij} is symmetric,

$$\rho_{14} = \rho_{41}, \quad \rho_{23} = \rho_{32}, \tag{B10}$$

therefore,

$$\rho_{ij} = \begin{pmatrix} \rho_{11} & 0 & 0 & \rho_{14} \\ 0 & \rho_{22} & \rho_{23} & 0 \\ 0 & \rho_{32} & \rho_{33} & 0 \\ \rho_{41} & 0 & 0 & \rho_{44} \end{pmatrix}. \tag{B11}$$

3. Building the reduced density matrix

The available code of partial trace involves permutating rows or columns of the density matrix ρ. On one hand, we need to avoid generating the huge matrix ρ (2^{19} by 2^{19}). On the other hand, even if we have ρ, permutations are too costly to be computed. Fortunately, we are able to convert "generate a global density matrix, then partial trace" into "get six elements then build a reduced density matrix." These six elements are closely related to the ground state, which we have already obtained after the application of Tracemin. In fact, the structure of the system (the Hamiltonian) guarantees that our ground state is a real vector and implicit of time. That makes the calculation neater, with no worry about the complex conjugate and time evolution.

Here is how to retreat the six elements. For example, we are intent on tracing three spins: first, third, and fifth, out of a total five, provided a ground state with the above properties. We start from the definition of partial trace [Eq. (B4)],

$$\begin{aligned}&\langle u_n(2)|\langle v_p(4)|\rho(2,4)|u_{n'}(2)\rangle|v_{p'}(4)\rangle\\&\quad=\sum_{\alpha,\beta,\gamma}\langle a_\alpha(1)|\langle u_n(2)|\langle b_\beta(3)|\langle v_p(4)|\langle c_\gamma(5)|\psi\rangle\\&\qquad\times\langle\psi|a_\alpha(1)\rangle|u_{n'}(2)\rangle|b_\beta(3)\rangle|v_{p'}(4)\rangle|c_\gamma(5)\rangle,\end{aligned}\tag{B12}$$

and carry it out for a specific matrix element

$$\begin{aligned}&\rho_{11}(2,4)\\&\quad=\langle 00|\rho(2,4)|00\rangle\\&\quad=\sum_{\alpha,\beta,\gamma}\langle\underline{a_\alpha(1)}\,\underline{0}\,\underline{b_\beta(3)}\,\underline{0}\,\underline{c_\gamma(5)}|\psi\rangle\langle\psi|\underline{a_\alpha(1)}\,\underline{0}\,\underline{b_\beta(3)}\,\underline{0}\,\underline{c_\gamma(5)}\rangle\\&\qquad\because|\psi\rangle\text{ is real}\\&\quad=\sum_{\alpha,\beta,\gamma}\langle\underline{a_\alpha(1)}\,\underline{0}\,\underline{b_\beta(3)}\,\underline{0}\,\underline{c_\gamma(5)}|\psi\rangle^2.\end{aligned}\tag{B13}$$

Since

$$|\psi\rangle=\sum_{\alpha,n,\beta,p,\gamma}\psi_m|a_\alpha(1)u_n(2)b_\beta(3)v_p(4)c_\gamma(5)\rangle,\tag{B14}$$

$$\langle a_\alpha(1)u_n(2)b_\beta(3)v_p(4)c_\gamma(5)|\psi\rangle=\psi_m,\tag{B15}$$

$\langle\underline{a_\alpha(1)}\,\underline{0}\,\underline{b_\beta(3)}\,\underline{0}\,\underline{c_\gamma(5)}|\psi\rangle$ is the coefficient in front of base $|\underline{a_\alpha(1)}\,\underline{0}\,\underline{b_\beta(3)}\,\underline{0}\,\underline{c_\gamma(5)}\rangle$ at $|\psi\rangle$ expansion. When we write $|\psi\rangle$ as a column vector

$$\begin{pmatrix}\psi_1\\\psi_2\\\vdots\\\psi_{2^N}\end{pmatrix},$$

its elements are the coefficients corresponding to the basis

$$\begin{matrix}|00000\rangle\\|00001\rangle\\\vdots\\|11111\rangle\end{matrix}.$$

Then if we can locate $|\underline{a_\alpha(1)}\,\underline{0}\,\underline{b_\beta(3)}\,\underline{0}\,\underline{c_\gamma(5)}\rangle$ as the mth base among all bases, we know that $\langle\underline{a_\alpha(1)}\,\underline{0}\,\underline{b_\beta(3)}\,\underline{0}\,\underline{c_\gamma(5)}|\psi\rangle=\psi_m$. Our task is to locate all the bases with the second and fourth spins being at state $|0\rangle$, then pick out corresponding ψ_m's, and square and sum them together.

Before we continue onto the details, let us construct a basis matrix of five spins illustrated in Fig. 13 and define the following.

Period. We say the pattern like

$$\begin{matrix}0\\\vdots\\0\\1\\\vdots\\1\end{matrix}$$

is a period.

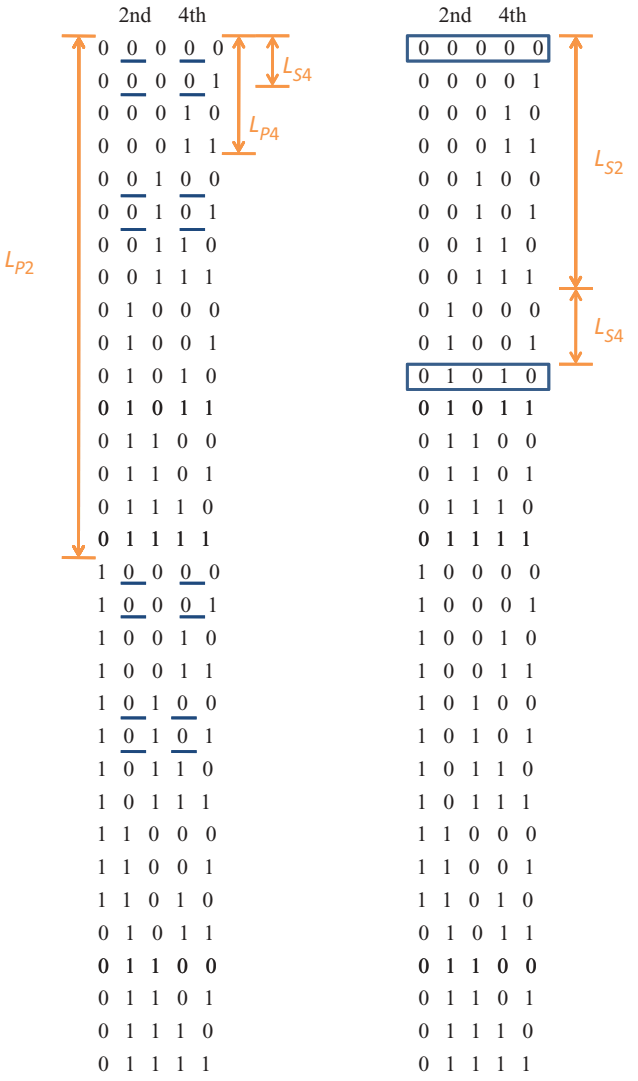

FIG. 13. (Color online) Illustration of the five-spins basis.

Segment.

$$\begin{matrix}0&1\\\vdots&\text{or}\ \vdots\\0&1\end{matrix}$$

is a segment.

Length. The number of elements in a period or a segment.

$L_{p\,i\text{th}}$. Length of a period of the ith spin.

$L_{s\,i\text{th}}$. Length of a segment of the ith spin.

The ith spin out of total N spins has

	ith/N	2nd/5	4th/5
L_P	2^{N-i+1}	$2^{5-2+1}=16$	$2^{5-4+1}=4$
L_S	2^{N-i}	$2^{5-2}=8$	$2^{5-4}=2$
No. of periods	2^{i-1}	$2^{2-1}=2$	$2^{4-1}=8$
No. of segments	2^i	$2^2=4$	$2^4=16$

Using these definitions, we can in general easily locate bases such as $|\ldots0\ldots0\ldots\rangle$, and within five steps obtain element $\rho_{11}(i,j)$, by applying the following algorithm.

1. First 0 in every period for ith spin is located at "p"$=1,\ 1+L_{p\,i\text{th}},\ 1+2L_{p\,i\text{th}},\ldots\leqslant 2^N$

2. First 0 in every period for jth spin, when the ith is 0, is located at "q" $= p,\ p + L_{p\,j\text{th}},\ 1 + 2L_{p\,i\text{th}}, \ldots \leqslant p + L_{p\,i\text{th}} - 1, (\because i < j\ \therefore L_{p\,jth} < L_{p\,i\text{th}} + L_{s\,jth} < L_{p\,i\text{th}})$.

3. $L_{s\,j\text{th}}$ decides the length of continued $|\ldots 0\ldots 0\ldots\rangle$ basis.

4. After locating "q," we naturally have $\psi(q) \Rightarrow \psi^2(q) \Rightarrow \psi^2(q) + \psi^2(q+1) + \ldots\ \psi^2(q + L_{s\,j\text{th}} - 1)$, then locate the next "$q$."

5. When we add them altogether, it is $\rho_{11}(i, j)$.

Similarly, we can locate "01" "10" "11" for

$$\rho_{22}(i, j) = \langle 01|\rho(i, j)|01\rangle, \tag{B16}$$

$$\rho_{33}(i, j) = \langle 10|\rho(i, j)|10\rangle, \tag{B17}$$

$$\rho_{44}(i, j) = \langle 11|\rho(i, j)|11\rangle. \tag{B18}$$

$\rho_{14}(i, j)$ and $\rho_{23}(i, j)$ are a bit different.

$$\rho_{14}(i, j) = \langle 00|\rho(i, j)|11\rangle = \langle \ldots 0\ldots 0\ldots|\psi\rangle\langle\psi|\ldots 1\ldots 1\ldots\rangle. \tag{B19}$$

In this case we do not have to locate $|\ldots 0\ldots 0\ldots\rangle$ & $\ldots 1\ldots 1\ldots\rangle$, respectively. Letting q be the position of $\ldots 0\ldots 0\ldots$ and the corresponding q' of $\ldots 1\ldots 1\ldots$ (i.e., other bases are the same); they are related by $q' = q + L_{s\,i\text{th}} + L_{s\,j\text{th}}$. That enables us to obtain ρ_{11} and ρ_{14} at the same time:

$$\rho_{11}(i, j) = \sum \psi^2(q), \tag{B20}$$

$$\rho_{14}(i, j) = \sum \psi(q)\psi\left(q + L_{s\,i\text{th}} + L_{s\,i\text{th}}\right). \tag{B21}$$

[1] A. Amico, R. Fazio, A. Osterloh, and V. Vedral, Rev. Mod. Phys. **80**, 517 (2008).

[2] C. H. Bennett and D. P. DiVincenzo, Nature **404**, 247 (2000).

[3] C. Macchiavello, G. M. Palma, and A. Zeilinger, *Quantum Computation and Quantum Information Theory* (World Scientific, Hackensack, 2000).

[4] M. Nielsen and I. Chuang, *Quantum Computation and Quantum Communication* (Cambridge University Press, Cambridge, 2000).

[5] J. Gruska, *Quantum Computing* (McGraw-Hill, New York, 1999).

[6] V. Vedral, M. B. Plenio, M. A. Rippin, and P. L. Knight, Phys. Rev. Lett. **78**, 2275 (1997).

[7] Y. Pashkin, T. Tilma, D. Averin, O. Astafiev, T. Yamamoto, Y. Nakamura, F. Nori, and J. Tsai, Int. J. Quantum. Inform. **1**, 421 (2003).

[8] K. Maruyama, T. Iitaka, and F. Nori, Phys. Rev. A **75**, 012325 (2007).

[9] A. Osterloh, L. Amico, G. Falci, and R. Fazio, Nature **416**, 608 (2002).

[10] T. Osborne and M. A. Nielsen, Phys. Rev. A **66**, 032110 (2002).

[11] A. Osterloh, L. Amico, F. Plastina, and R. Fazio, in *Proceedings of SPIE Quantum Information and Computation II*, *Bellingham, 2004*, edited by E. Donkor, A. R. Pirich, and H. E. Brandt (SPIE, Bellingham, 2004), Vol. 5436, p. 150.

[12] G. Vidal, J. I. Latorre, E. Rico, and A. Kitaev, Phys. Rev. Lett. **90**, 227902 (2003).

[13] L. A. Wu, M. S. Sarandy, and D. A. Lidar, Phys. Rev. Lett. **93**, 250404 (2004).

[14] L. A. Wu, M. S. Sarandy, D. A. Lidar, and L. J. Sham, Phys. Rev. A **74**, 052335 (2006).

[15] V. Akulin, G. Kurizki, and D. A. Lidar, J. Phys. B **40**, E01 (2007).

[16] D. A. Lidar, A. T. Rezakhani, and A. Hamma, J. Math. Phys. **50**, 102106 (2009).

[17] O. Osenda, Z. Huang, and S. Kais, Phys. Rev. A **67**, 062321 (2003).

[18] Z. Huang, O. Osenda, and S. Kais, Phys. Lett. **A322**, 137 (2004).

[19] Z. Huang and S. Kais, Int. J. Quantum. Inform. **3**, 483 (2005).

[20] Z. Huang and S. Kais, Phys. Rev. A **73**, 022339 (2006).

[21] S. Kais, Adv. Chem. Phys. **134**, 493 (2007).

[22] A. Sandvik and J. Kurkijärvi, Phys. Rev. B **43**, 5950 (1991).

[23] O. F. Syljuåsen and A. W. Sandvik, Phys. Rev. E **66**, 046701 (2002).

[24] O. F. Syljuåsen, Phys. Lett. **A322**, 25 (2003).

[25] O. F. Syljuåsen, Phys. Rev. A **68**, 060301 (2003).

[26] A. Sameh and J. A. Wisniewski, SIAM J. Numer. Anal. **19**, 1243 (1982).

[27] A. Sameh and Z. Tong, J. Comput. Appl. Math. **123**, 155 (2000).

[28] G. Sleijpen and H. van der Vorst, SIAM J. Matrix Anal. Appl. **17**, 401 (1996).

[29] W. K. Wootters, Phys. Rev. Lett. **80**, 2245 (1998).

[30] V. Coffman, J. Kundu, and W. K. Wootters, Phys. Rev. A **61**, 052306 (2000).

[31] T. J. Osborne and F. Verstraete, Phys. Rev. Lett. **96**, 220503 (2006).

[32] C. Cohen-Tannoudji, B. Diu, and F. Laloe, *Quantum Mechanics* (Wiley Interscience, New York, 2006).

[33] K. Penson, R. Jullien, and P. Pfeuty, Phys. Rev. B **25**, 1837 (1982).

[34] C. Hamer, J. Phys. A: Math. Gen. **33**, 6683 (2000).

[35] S. Kais and P. Serra, Adv. Chem. Phys. **125**, 1 (2003).

[36] P. Serra, A. F. Stanton, and S. Kais, Phys. Rev. E **55**, 1162 (1997).

[37] S. Sachdev, *Quantum Phase Transitions* (Cambridge University Press, Cambridge, 1999).